Search › Results for Altuntas I* (Auth... › Experimental insights toward carrier localization in in-rich InGaAs/InP as ca...

Full text at publisher | Export | Add To Marked List

Experimental insights toward carrier localization in in-rich InGaAs/InP as candidate for SWIR detection: Microstructural analysis combined with optical investigation

By Ben Arbia, M (Ben Arbia, Marwa) [1] ; Demir, I (Demir, Ilkay) [2] ; Kaur, N (Kaur, Navpreet) [3] ; Saidi, F (Saidi, Faouzi) [1] , [4] ; Zappa, D (Zappa, Dario) [3] ; Comini, E (Comini, Elisabetta) [3] ; Altuntas, I (Altuntas, Ismail) [2] ; Maaref, H (Maaref, Hassen) [1]

View Web of Science ResearcherID and ORCID (provided by Clarivate)

Source MATERIALS SCIENCE IN SEMICONDUCTOR PROCESSING

Volume: 153

DOI: 10.1016/j.mssp.2022.107149

Article Number 107149

Published JAN 2023

Early Access OCT 2022

Indexed 2023-03-29

Document Type Article

Abstract

Hyperspectral imaging has been flourished thanks to the huge investigation of the infrared spectrum from NIR to LWIR bands. The ternary InGaAs has been investigated herein in the context of studying the structural de-pendences of localization phenomenon by X-ray diffraction (XRD), scanning electron microscopy-energy dispersive X-ray (SEM-EDX), Raman, ultraviolet-visible (UV-vis), and photoluminescence (PL) techniques. Using metal-organic vapor phase epitaxy (MOVPE), we succeed to grow the InGaAs directly on InP substrate at 560 degrees C as an active layer with indium concentration exceeding the "golden" value (53%) to enlarge its cutoff absorption wavelength. X-ray diffraction proved a good crystallinity of the heterostructure with a sharp peak related to the thick substrate and another peak attributed to the thin layer of InGaAs. Moreover, an interfacial layer appeared at the logarithmic scale of XRD patterns and was confirmed by Raman analysis. The SEM-EDX revealed an average indium concentration (62%), almost the growth concentration. However, a cross-section compositional profile over the heterostructure showed an inhomogeneous distribution of the indium. This is predictable from the composition fluctuation in the indium-containing alloys and the volatility (surface segre-gation) of As (In). On the other side, the optical investigation of InGaAs demonstrated an anomalous behavior of luminescence versus temperature, manifested by the S-shape feature. This trend stems from the potential fluc-tuation induced by the non-uniform distribution of indium. A numerical simulation was developed based on the localized state ensemble (LSE) model to well-reproduce this anomaly by giving the best fitting parameters and comparing them with those calculated using the semi-empirical models (Vin similar to a and Pa center dot ssler). The results reported here will help in optimizing the epitaxy design of future InGaAs/InP and further studying its surface morphology and device performance.

Keywords

Author Keywords: InGaAs; InP; X-ray diffraction; SEM-EDX; Raman; Temperature dependent photoluminescence; (TDPL); Carrier localization

Keywords Plus: MOLECULAR-BEAM EPITAXY; QUANTUM-WELLS; TEMPERATURE-DEPENDENCE; INTERFACE ABRUPTNESS; RAMAN-SPECTROSCOPY; GROWTH; PHOTOLUMINESCENCE; SUPERLATTICES; HETEROSTRUCTURE; LUMINESCENCE

Journal information

MATERIALS SCIENCE IN SEMICONDUCTOR PROCESSING

Publisher name: ELSEVIER SCI LTD

Journal Impact Factor ™

4.1 (2022) | 3.7 (Five Year)

JCR Category	Category Rank	Category Quartile
ENGINEERING, ELECTRICAL & ELECTRONIC *in SCIE edition*	97/275	Q2
MATERIALS SCIENCE, MULTIDISCIPLINARY *in SCIE edition*	139/344	Q2
PHYSICS, APPLIED *in SCIE edition*	45/160	Q2
PHYSICS, CONDENSED MATTER *in SCIE edition*	21/67	Q2

Source: Journal Citation Reports 2022. Learn more

Journal Citation Indicator ™

0.91 (2022) | 0.92 (2021)

JCI Category	Category Rank	Category Quartile
ENGINEERING, ELECTRICAL & ELECTRONIC *in SCIE edition*	106/352	Q2
MATERIALS SCIENCE, MULTIDISCIPLINARY *in SCIE edition*	118/424	Q2
PHYSICS, APPLIED *in SCIE edition*	42/178	Q1
PHYSICS, CONDENSED MATTER *in SCIE edition*	16/76	Q1

The Journal Citation Indicator is a measure of the average Category Normalized Citation Impact (CNCI) of citable items (articles and reviews) published by a journal over a recent three year period. It is used to help you evaluate journals based on other metrics besides the Journal Impact Factor (JIF).

Learn more

Materials Science in Semiconductor Processing 159 (2023) 107389

Contents lists available at ScienceDirect

Materials Science in Semiconductor Processing

journal homepage: www.elsevier.com/locate/mssp

InGaAs-based Gunn light emitting diode

G. Kalyon [a], S. Mutlu [a], F. Kuruoglu [a], I. Pertikel [b], I. Demir [b], A. Erol [a,*]

[a] Department of Physics, Faculty of Science, Istanbul University, Vezneciler, 34134, Istanbul, Turkey
[b] Sivas Cumhuriyet University, Nanophotonics Research and Application Center, 58140, Sivas, Turkey

ARTICLE INFO

Keywords:
Gunn diode
Light emitting diode
InGaAs
Gunn oscillations
Gunn domain

ABSTRACT

We report an n-type $In_{0.53}Ga_{0.47}As$ based Gunn light emitting diode operated at around 1.6 μm. The device structure comprises of an n-type $In_{0.53}Ga_{0.47}As$ epilayer with a thickness of 5 μm grown by Metal Organic Vapour Phase Epitaxy (MOVPE) on a semi-insulating InP substrate and fabricated in a planar architecture with a stepped structure at anode side to suppress the destructive effect of high built-in electric field in propagating Gunn domain. Gunn diode is operated under pulsed voltage with a pulse width of 60 ns and pulse duration of 4.5 ns to keep the duty cycle as low as 0.0013%. The Gunn oscillations with an 1 ns period are observed at around 4.1 kV/cm, which corresponds to the electric field threshold of Negative Differential Resistance (NDR). The light emission at around 1.6 μm also starts at the threshold electric field of the NDR region (E = 4.2 kV/cm) of the current-voltage curve, and the emission intensity increases drastically with increasing applied electric field. The observed light emission at NDR threshold electric field where Gunn oscillations appear on the voltage pulse is attributed to the impact ionisation process occurring in the current domains along the sample, which generates excess carriers to initiate the band-to-band recombination in $In_{0.53}Ga_{0.47}As$.

1. Introduction

Gunn oscillations were first observed by Gunn as an instability in the current in the form of an oscillations on the normal pulse current under an applied pulsed electric field at around 3 kV/cm was applied to an n-type GaAs [1]. Gunn reported that without needing a p-n junction structure and inconveniently small dimensions, these oscillations were produced from just a piece of n-type material, so-called Gunn oscillations could be a cheaply manufacturing to fabricate devices operating in microwave regions at room temperature. Since Gunn's invention, the Gunn diode, whose operation is based on Gunn oscillations has been playing an important role to generate microwave power in the GHz frequency range [2–5]. Gunn diode is a two terminal NDR device consisted of just one type of doped III-V semiconductor. First Gunn diode was fabricated from an n-type GaAs [6], then other III-V materials such as InP [7], InGaAs [2,4,8–10], GaN [8,9], etc. were reported as the active region of Gunn diode. In the beginning, a great effort has been spent to fabricate robust devices since the built-in electric field in Gunn domains can become as large as to damage the device as propagating Gunn domain from the cathode towards to the anode. Different anode structures such as dumb-bell contact [2,10–12], wedge [13,14], axis off from the cathode [14], and Schottky contact at the anode region instead of Ohmic contact [10,11,15] have been fabrication strategies to minimise the amplitude of the built-in electric field at the anode of the device. From an electronic point of view, following robust and stable oscillations the motivation was focused on increasing the frequency of Gunn oscillations towards to THz region because of the wide range of important applications in the THz region [12,16]. In a recent theoretical study, it has been revealed that Gunn diodes can be operated above 1 THz with a proper design of the device [17]. On the other hand, considering experimental studies, the frequency values of Gunn oscillations are still below 1 THz but have approached to 1 THz in a recent study on a notch δ doped GaAs-based Gunn diodes [18].

While an effort has been spending to enlarge the upper frequency limit of the Gunn diode towards to THz region, from an optical point of view, light emission from a travelling high-field Gunn domain was first observed by Southgate from GaAs in 1967 [19]. Long after this observation, Balkan et al. reported light emission (electroluminescence, EL) from n-type GaAs and $Al_xGa_{1-x}As$ -based devices with a various lengths between 4 μm and 316 μm [20]. Chung et al. have presented an evaluation of a simple GaAs-based Gunn diode based light emitter towards to Fabry Perot laser [21] and then vertical cavity light emitting laser (VCSEL) emitting in the 830–850 nm wavelength ranges [22] at 90 K [22]. In a recent study of us, we have presented edge and surface light

* Corresponding author.
E-mail address: ayseerol@istanbul.edu.tr (A. Erol).

https://doi.org/10.1016/j.mssp.2023.107389
Received 4 December 2022; Received in revised form 5 February 2023; Accepted 7 February 2023
Available online 14 February 2023

emission from an AlGaAs-based Gunn diode and a Fabry-Perot AlGaAs-based Gunn diode emitting around 816 nm at room temperature [17]. The observed EL from the Gunn diode is associated with the band to band recombination of non-equilibrium electron-hole pairs generated via impact ionisation process in the propagating Gunn domains when the Gunn diode is operated in the NDR regime.

In this paper, we demonstrate an n-type $In_{0.53}Ga_{0.47}As$-based Gunn light emitting diode fabricated in a planar architecture at around 1.6 μm at room temperature under pulsed operation. Gunn oscillations with a frequency of 1 GHz are observed at threshold of NDR as well as light emission at around 1.6 μm starts. The light emission from the Gunn diode does not dependent on applied voltage polarity. EL intensity enhances as increasing applied electric field above the NDR threshold. Integrated EL intensity exhibits a drastic increase above the NDR threshold.

2. Experimental details

The investigated Gunn device structure was grown on a semi-insulating InP substrate by MOVPE. In order to prevent undesired defects from the substrate surface from advancing into the grown layer and to prepare a more flexible environment for growth, firstly homoepitaxial growth is usually performed on the substrate. In this study, approximately 300 nm thick InP buffer layer was grown on semi-insulating InP (SI–InP). For the InP buffer layer, high purity trimethylindium (TMIn, In $(CH_3)_3$) metalorganic compound and phosphine (PH_3) hydride were utilised as In and P sources, respectively. The flow values of TMIn and PH_3 for growing buffer layer were 160 sccm and 200 sccm, respectively. After the InP buffer layer was successfully grown, the doped $In_xGa_{1-x}As$ layer was grown. For InGaAs layer, high purity TMIn and trimethylgallium (TMGa, $Ga(CH_3)_3$) metalorganic compounds were used as In and Ga sources, and arsine (AsH_3) hydride was used as As source. SiH_4 gas, which is a hydride source was used for n-type doping. In addition, ultra-high purified hydrogen (H_2) was used as a carrier gas. The growth parameters for the InGaAs layer are as follows: the growth temperature is 650 °C, and the TMIn, TMGa, AsH_3 and SiH_4 flows are 190 sccm, 6 sccm, 200 sccm and 0.24 sccm, respectively.

X-ray diffraction (XRD) θ-2θ scan was performed to understand the crystal quality of the grown sample and to determine the ternary alloy ratios. After the XRD measurement, the alloy ratio of the grown sample was determined by the Global Fit simulation software. The In concentration in the $In_xGa_{1-x}As$ alloy was determined as $x = 0.53$. The measurement and simulation results are given in Fig. 1. In this graph, the blue curve corresponds to the measurement result and the black curve to the simulation result. In order to obtain comprehensive and accurate information from grown samples, the match between simulation and measurement must be considered. The measurement result and the simulation result overlapped. The full width at half maximum (FWHM) of the XRD peak was determined as 173 arcsec. This value indicates that the grown sample has good crystal quality.

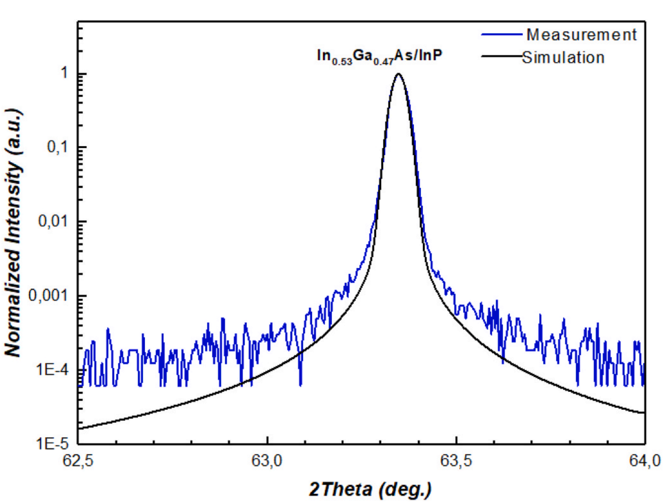

Fig. 1. Simulation (black solid line) and XRD θ-2θ measurement (blue solid line) for the sample.

By choosing the In alloy concentration of 0.53 in the 5 μm thick InGaAs epilayer forming the active region of the Gunn device, a perfect lattice match with the semi-insulating InP substrate was achieved. $In_{0.53}Ga_{0.47}As$ epilayer thickness was designed to be greater than the electromagnetic wavelength to be emitted by the Gunn device. Therefore, the interference effect of the Gunn device emission due to the inner reflections is suppressed. The epilayer $In_{0.53}Ga_{0.47}As$ was doped by Si atoms with a density of 5×10^{16} cm^{-3}. A schematic layer structure of the device is given in Fig. 2.

The sample was defined in Hall Bar geometry and planar simple bar architecture with a stepped geometry at the anode side using standard photolithography techniques for Hall Effect and electroluminescence (EL) measurements, respectively. The samples were etched approximately 5 μm down through the $In_{0.53}Ga_{0.47}As$ layer to pattern Hall bar and mesa geometry using wet etching with $C_6H_8O_7/H_2O_2$ (citric acide/hydrogen peroxide: 5/1) solution. To convert the mesa geometry to the stepped planar simple bar, one edge of the mesa was further etched 4 μm. Prior to metal deposition, the samples were kept in a plasma asher (Diener, ZEPTO) for 1 min to remove organic impurities on the surface. Au/Cr (100nm/10 nm) were used to have ohmic anode and cathode contacts. Samples were placed on a copper heat sink to minimise heating of the sample during the high electric field measurements then 25 μm diameter of gold wires were bonded to make them ready for electrical measurements using a wire bonder wedge mode (TPT, HB05). The details about $In_{0.53}Ga_{0.47}As$ – based Gunn device structure and contact configuration of the simple bar with step geometry are shown in Fig. 3.

As the Gunn domain propagates from cathode to anode, built-in electric field in the domain increase and can damage the device at the proximity of the anode, which is the main obstacle to obtaining stable Gunn oscillations and robust Gunn diodes. To avoid the breakdown of the device, different contact geometries were proposed [2,3,14,17,23]. Here, we propose a planar architecture with a stepped anode to decrease the electric field in the vicinity of anode. The electric field distribution along the samples was simulated using AC/DC module of the COMSOL Multiphysics program for both simple bar with/without step geometry. In a standard simple bar shape, since contact metals were evaporated on the surface and did not diffusied thorough the sample, a well-defined separation between metal and semiconductor are occurred, resulting in a sharp transition from metal contact area to semiconductor area. This sharp transition and corners cause a higher electric field as illustrated in Fig. 4a. To initiate a Gunn domain in the vicinity of cathode region, a higher electric field at cathode section is beneficial. However, as Gunn domain propagates along the anode, the built-in electric field increases and together with a drastically higher electric field around anode side (Fig. 4a) causes an uncontrollable increase of the excess carriers via impact ionisation then damaging of device. Using a simple bar with step geometry at the one end (anode) of the device suppresses the high electric field distribution. As increasing the step thickness electric field in this area becomes lower (Fig. 4b). COMSOL simulations are given in Fig. 5 for simple bar with/without step geometry to reveal the electric field distribution at around cathode and anode regions. It is clear that a uniform electric field is applied along the sample away from cathode and anode sections. The optimum step thickness was determined as 4 μm and the device were fabricated accordingly.

Hall Effect measurement to obtain the carrier concentration and the carrier mobility, and photoluminescence (PL) measurement to determine the band gap of $In_{0.53}Ga_{0.47}As$ were performed. High speed pulsed current-voltage (I–V) measurement was conducted to observe Gunn oscillations and to determine the threshold electric field for NDR. To find the threshold electric field that emission occurs, an integrated EL

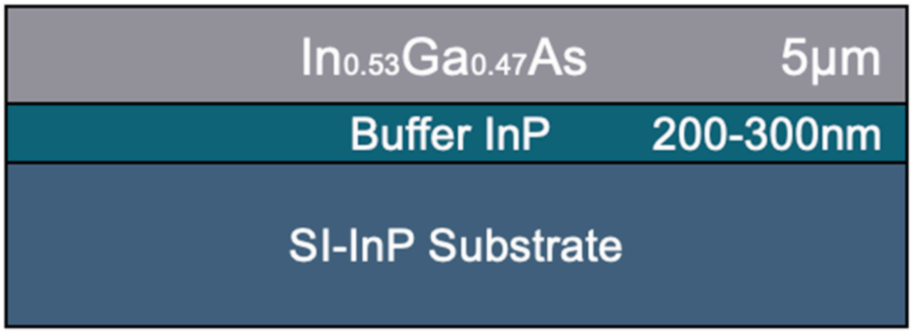

Fig. 2. A schematic structure of the Gunn device.

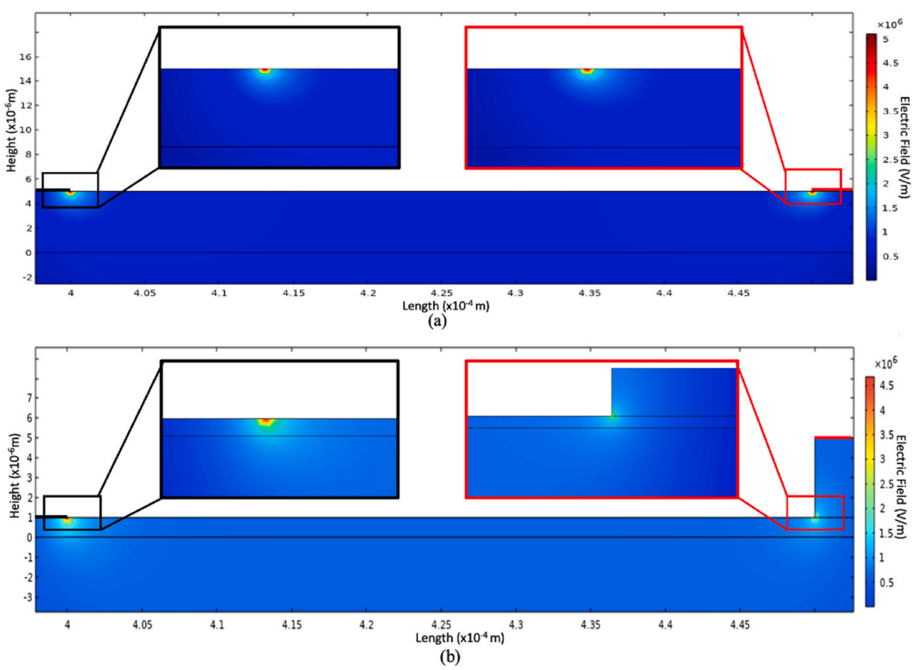

Fig. 3. $In_{0.53}Ga_{0.47}As$ – based Gunn device a) Fabricated Gunn device in a planar architecture stepped at anode, b) cross-section structure, c) top view of the contacts with their dimensions.

intensity-electric field measurement was carried out. Spectral EL measurements were performed to determine the light emission characteristic as a function of the applied electric field. All experiments were conducted with a free space all in one experimental set-up at room temperature given in Fig. 6.

Pulsed voltages of 60 ns duration were applied along the Gunn device using an Avtech AVR-Z5 high voltage pulse generator. In order to avoid Joule heating, a duty cycle was kept at less than %0.0015. Also, the repetition rate of the pulse is 4.5 ms (220 Hz). Applied, and sample voltages were measured by using a digital four channels Lecroy Wavepro z715 oscilloscope with a bandwidth of 1.5 GHz.

The emitted light from the Gunn device, which was operated at around NDR threshold electric field excited with pulsed voltage was dispersed by a 0.5 m focal length of monochromator. The dispersed light at the exit slit of the monochromator was collected and converted to the electrical signal using a photomultiplier tube (PMT, Hamamatsu, R5509) operated at 1500 V. The output of PMT was measured using Stanford Box-car Averager that is a suitable instrument to measure high speed pulsed electrical signals from 1 ns to 3 µs and at a maximum 20 kHz frequency.

3. Results and discussion

PL measurements at room temperature were made to determine the bandgap of the active layer ($In_{0.53}Ga_{0.47}As$) of the Gunn device. As seen in Fig. 7, the PL peak energy is 0.77 eV (1.6 µm), which is consistent with the bandgap of $In_{0.53}Ga_{0.47}As$. FWHM of the PL spectrum is 65 nm which was affected by the slit widths. Slit widths were kept at 1 mm.

Hall effect measurement was performed to determine the electron density and electron mobility in $In_{0.53}Ga_{0.47}As$. As a result of Hall effect measurement, electron density and electron mobility were found to be 3.41×10^{16} cm^{-3} and 8700 cm^2/V.s, respectively. The electron mobility value agrees with the reported value for $In_{0.53}Ga_{0.47}As$ doped with 2.75 $\times 10^{16}$ cm^{-3} as being 8600 cm^2/V.s by Kowalsky et al. [24].

Electric field dependence of electron drift velocity and integrated EL intensity $In_{0.53}Ga_{0.47}As$-based Gunn device are presented in Fig. 8. Drift velocity is obtained from current-voltage measurements and is defined as

$$V_d = \frac{I}{n.e.w.d} \quad (1)$$

where V_d is drift velocity, n 3D carrier density, I current, w channel width and d thickness of the sample. The applied electric field on the

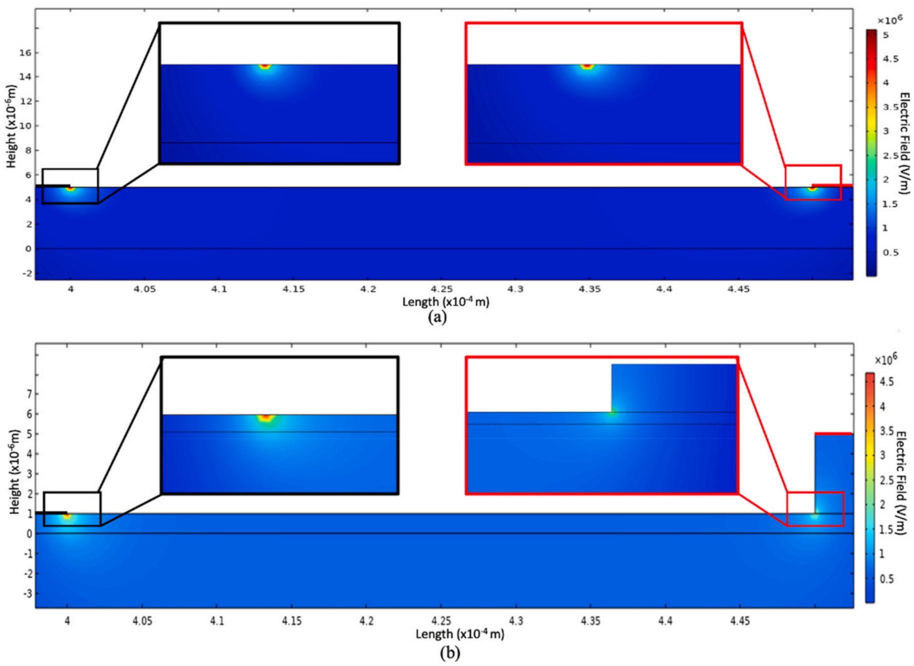

Fig. 4. COMSOL simulations for a) a simple bar b) a step geometry. The electric field distribution at cathode and anode sections are zoomed-in to give a better presentation of the simulation results. From red to blue areas, distribution of electric field changes from higher to lower values. Away from the cathode and anode sections, applied electric field distribution is uniform along the sample as shown in Fig. 5. .

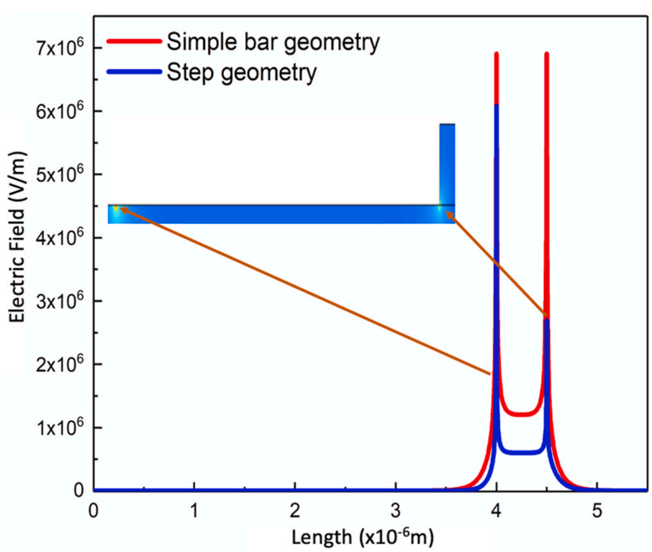

Fig. 5. Distribution of the electric field along the Gunn device.

sample is calculated using

$$E = \frac{V}{L} \quad (2)$$

where E is the electric field, V the applied voltage, and L the channel length. The saturation region and the onset of the NDR region were given on the drift velocity *versus* electric field curve. It shows ohmic characteristics in electric field values up to the saturation region (3 kV/cm) and NDR characteristic appears at around 3.5 kV/cm. The saturation velocity is 1.92×10^6 cm/s. The threshold of NDR for the $In_{0.53}Ga_{0.47}As$ with a carrier concentration of 2.75×10^{16} cm^{-3} is observed at 3.5 kV/cm by Kowalsk et al. [24]. Haase et al. examined the threshold electric field dependence on the carrier concentration, and they reported that the NDR's threshold value is approximately 3 kV/cm for the carrier concentration of 1×10^{16} cm^{-3}, which is similar to the electron density in our sample [25].

The threshold electric field for emission is determined from integrated EL *versus* electric field as 4.23 kV/cm. Above the threshold electric field the emission intensity drastically increases with the increasing electric field.

The Gunn oscillations on the voltage pulse measured from across the load resistance are shown in Fig. 9a at various electric fields, which are above the threshold of NDR. The drift velocity and Gunn oscillation measurements as a function of the electric field were also carried out with a simple bar geometry which validated the simulation results, and it was not exhibited Gunn oscillation as can be seen in Fig. S1 (Supplementary Information). This observed behaviour can be attributed to the current controlled NDR (S-type) mechanism [26] (Fig. S2) and, that is explained by a sudden increase in current due to the impact ionisation mechanism and the realization of the current-controlled NDR mechanism instead of the voltage-controlled NDR. In the S-type NDR mechanism, the current paths are emerged along the samlple length that damages the sample as can be seen in Fig. S3 instead of the observation of stable domains with the increasing electric field [19]. In Fig. 9b, the period and amplitude of Gunn oscillations are presented at different electric fields. When the applied electric field is increased, Gunn oscillations appear on the pulse at the onset of the NDR region that is originated from Gunn domain formation in the sample. Gunn domain propagates along the sample from the cathode to the anode without vanishing *via* an applied electric field until reaches the anode then a new domain is nucleated at the cathode again, resulting in Gunn oscillations [27]. The transit time of the domain from the cathode to the anode is found using

$$t_{tr} = L / V_d \quad (3)$$

where t_{tr}, L, and V_d are the transit time, sample length, and drift velocity, respectively. Domain transit time is calculated as 2.5 ns.

The built-in electric field in domain increases as applied electric field is increased. This increment results in an enhancement of the amplitude of the Gunn oscillations [14]. The period of Gunn oscillations is around 1 ns ($f = 1$ GHz) that is similar to the domain transit time (2.5 ns).

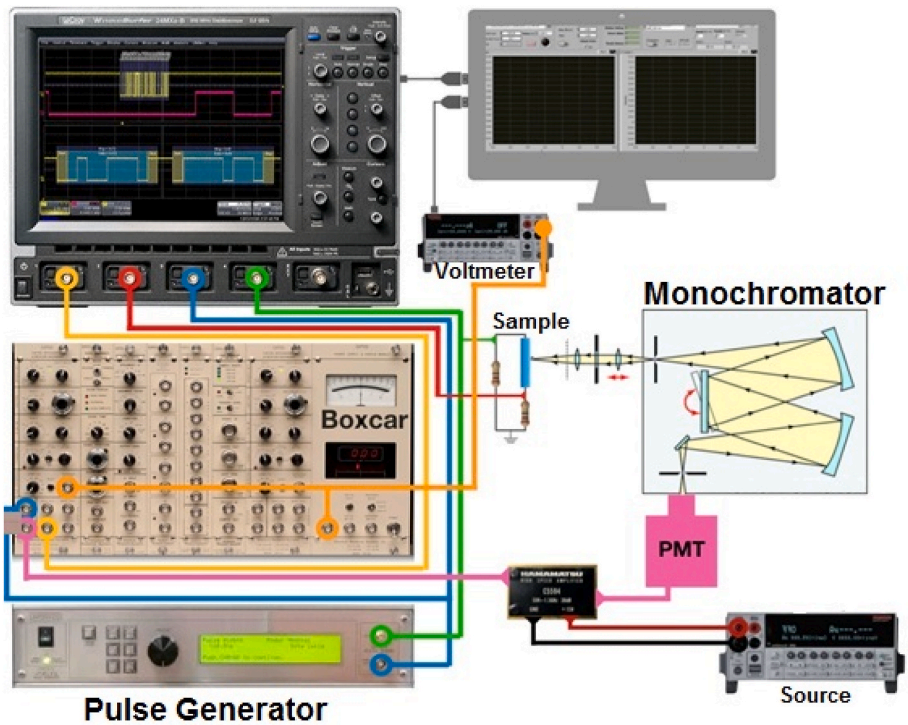

Fig. 6. All in one experimental setup.

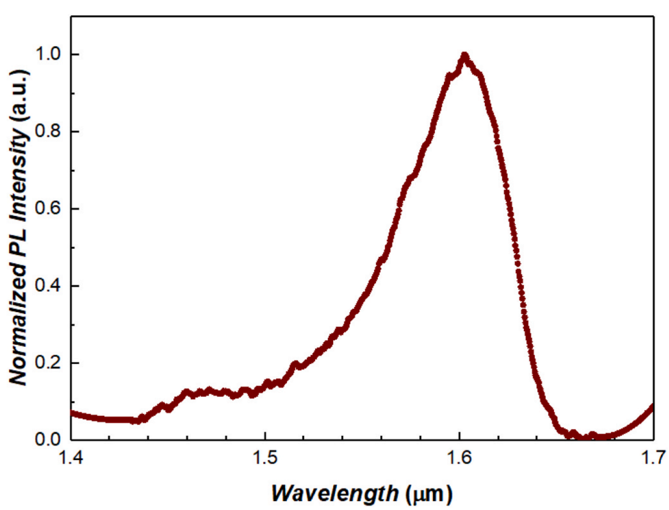

Fig. 7. PL spectrum at room temperature.

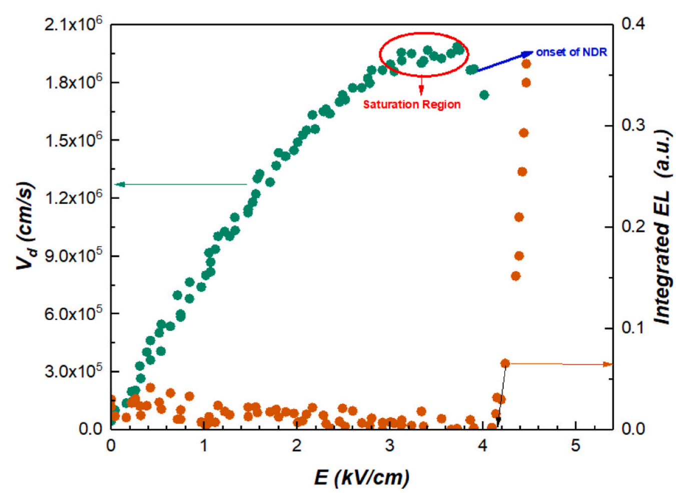

Fig. 8. Drift velocity and integrated EL *versus* applied electric field.

In n-type $In_{0.53}Ga_{0.47}As$-based Gunn device, a hole is generated in the valence band and two electrons are generated in the conduction band due to the impact ionisation originating from the domain transferred from the cathode to the anode. Generated excess electrons will release their energy by emitting photons, which corresponds to the bandgap of $In_{0.53}Ga_{0.47}As$. The carrier density caused by generated excess electrons in Gunn domain is obtained from Eq. (4),

$$n_{ex} = n_0.\alpha_e.L.\gamma.e^{-t_{tr}/\tau} \tag{4}$$

where n_{ex}, n_0, α_e, γ and τ are the excess carrier density, background electron density (doping density), impact ionisation coefficient, multiplication factor, and recombination lifetime, respectively.

To find the impact ionisation coefficient, domain electric field should be known. The domain electric field is determined by

$$E_d - E_R = \left[L.(E_A - E_R)\frac{2.e.n_0}{\varepsilon}\right]^{1/2} \tag{5}$$

where E_d, E_R, E_A and ε are the domain electric field, the electric field outside the domain, applied electric field above the NDR threshold and permittivity, respectively. The electric field outside of the domain is 3 kV/cm and above the NDR threshold applied electric field is 3.9 kV/cm. The domain electric field (E_d) is calculated as 200 kV/cm that is high enough to initiate impact ionisation in $In_{0.53}Ga_{0.47}As$. In the $In_{0.53}Ga_{0.47}As$ device, the impact ionisation coefficient is 1350 cm^{-1} at 200 kV/cm [28].

To calculate recombination lifetime, the $n_{ex} = n_{ex}(0) = n_0$ approximation is made [29]. $n_{ex}(0)$ is the initial carrier concentration. With this approach, the recombination lifetime is found to be 200 ns for a carrier concentration of 3.41×10^{16} cm^{-3}.

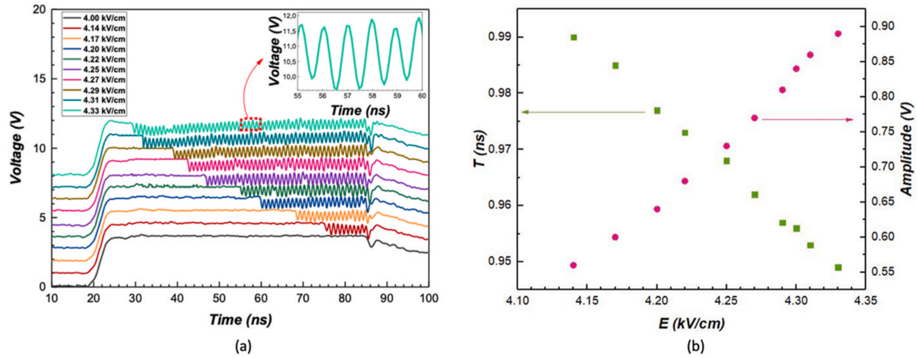

Fig. 9. a) Formation of Gunn oscillations for the various electric field and b) electric field dependence of the period and amplitude of Gunn oscillations.

The multiplication factor (γ) is found by multiplying oscillation frequency and pulse duration. When the excess carrier density, fundamental electron density, pulse ionisation coefficient, multiplicative factor and recombination lifetime values are used in Eq. (4), the excess carrier concentration (n_{ex}) generated via impact ionisation in Gunn domain is found as 1.4×10^{19} cm^{-3}. At 1.4×10^{19} cm^{-3} excess carrier concentration in Gunn domain, the recombination lifetime of excess carriers is found to be 0.065 ns. EL spectra for different electric field values at room temperature are given in Fig. 10 together with hot electron temperature. The hot electron temperature values determined from the high energy tail of the EL spectrum of the Gunn device increase as electric field is increased as given in the inset of Fig. 10. The peak energy of the EL spectrum corresponds to the bandgap of the n-type $In_{0.53}Ga_{0.47}As$ (0.77 eV). As increasing electric field, the intensity of the emission enhances.

Applied high electric fields heats the electrons above lattice temperature (hot electrons) in the Γ valley of InGaAs. The hot electron temperature can be found using the slope of the logarithm of EL intensity *versus* photon energy at the high energy tail side of the EL spectrum [30].

$$I_{EL} \propto exp(h\nu / k_B T_e) \quad (6)$$

where I_{EL}, $h\nu$, k_B and T_e are the EL intensity, emitted photon energy, Boltzmann constant and hot electron temperature, respectively.

There is another method for calculating electron temperature when the energy relaxation time is known [27] given by

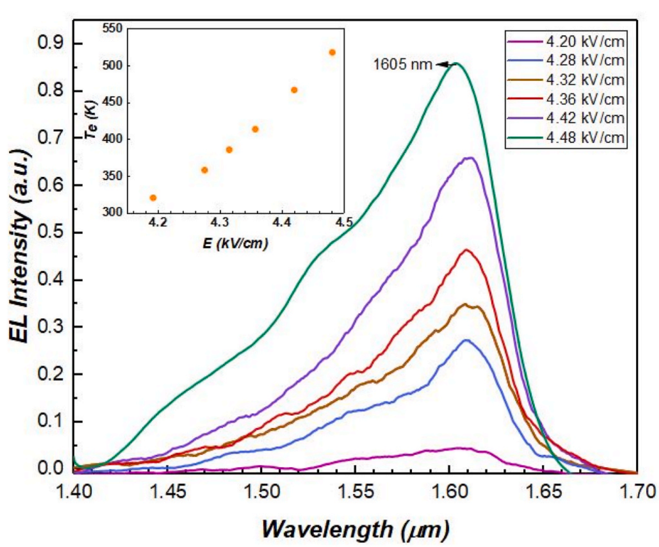

Fig. 10. EL spectrum at various electric field above NDR threshold. The inset shows the electric field dependence of hot electron temperature calculated from the EL spectrum's high energy tail.

$$q.V_d.E = \frac{3.k_B.(T_e - T)}{2\tau_e} \quad (7)$$

where V_d, E, k_B, T_e and T are the drift velocity, applied electric field, Boltzmann constant, electron temperature and lattice temperature respectively. τ_e is taken 10^{-12} s in InGaAs [27]. Using the drift velocity *versus* electric field graph in Fig. 8, the drift velocity corresponding to the electric field value of 4.48 kV/cm is 4.35×10^6 cm/s. When the values are used in Eq. (7), the electron temperature is calculated as 510 K at an electric field value of 4.48 kV/cm. For the given electric field value, the electron temperature calculated from the EL spectrum is 520 K. The results show that electron temperatures which calculated by these two methods are in good agreement.

4. Conclusions

In this study, we have demonstrated an $In_{0.53}Ga_{0.47}As$ -based Gunn light emitting diode. The emission characteristic has been investigated as a function of applied electric field at around NDR regime where Gunn oscillations are observed. The integrated EL has started at an electric field of 4.23 kV/cm, and the emission intensity drastically increases as electric field is increased. The period of Gunn oscillations and the domain transition time are found to be 1 ns, and 2.5 ns, respectively. EL reveals that the emission wavelength is 1.6 μm and the EL intensity and electron temperature increase with increasing electric field.

Our results have revealed that $In_{0.53}Ga_{0.47}As$ -based Gunn light emitting diode is an alternative to conventional p-n junction diode-based light emitters with its simpler and cost-effective design consisted of piece of just one type of doped semiconductor and Ohmic contacts, voltage polarity-independent operation and providing that the device has been appropriately engineered.

CRediT authorship contribution statement

G. Kalyon: Writing – original draft, Validation, Investigation, Formal analysis. **S. Mutlu:** Writing – original draft, Validation, Investigation, Formal analysis. **F. Kuruoglu:** Writing – review & editing, Formal analysis. **I. Pertikel:** Writing – original draft, Resources. **I. Demir:** Writing – original draft, Resources. **A. Erol:** Writing – original draft, Supervision, Project administration, Funding acquisition.

Declaration of competing interest

The authors declare that they have no known competing financial interests or personal relationships that could have appeared to influence the work reported in this paper.

Data availability

Data will be made available on request.

Acknowledgments

This work is supported by TUBITAK (Project number: 120F062) and the Scientific Research Projects Coordination Unit of Istanbul University (Project Numbers: FYL-2022-38329 and FBG-2022-38573).

Appendix A. Supplementary data

Supplementary data to this article can be found online at https://doi.org/10.1016/j.mssp.2023.107389.

References

[1] J.B. Gunn, Microwave oscillations of current in lll-V semiconductors, Solid State Commun. 88 (1963) 88–91.
[2] C. Li, A. Khalid, S.H. Paluchowski Caldwell, M.C. Holland, G.M. Dunn, I.G. Thayne, D.R.S. Cumming, Design, fabrication and characterization of $In_{0.23}Ga_{0.77}As$-channel planar Gunn diodes for millimeter wave applications, Solid State Electron. 64 (2011) 67–72, https://doi.org/10.1016/j.sse.2011.07.008.
[3] M. Montes, G. Dunn, A. Stephen, A. Khalid, C. Li, D. Cumming, C.H. Oxley, R. H. Hopper, M. Kuball, Reduction of impact ionization in GaAs-based planar Gunn diodes by anode contact design, IEEE Trans. Electron. Dev. 59 (2012) 654–660, https://doi.org/10.1109/TED.2011.2177094.
[4] A. Khalid, C. Li, V. Papageogiou, G.M. Dunn, M.J. Steer, I.G. Thayne, M. Kuball, C. H. Oxley, M. Montes Bajo, A. Stephen, J. Glover, D.R.S. Cumming, $In_{0.53}Ga_{0.47}As$ planar gunn diodes operating at a fundamental frequency of 164 GHz, IEEE Electron. Device Lett. 34 (2013) 39–41, https://doi.org/10.1109/LED.2012.2224841.
[5] Kroemer Herbert, Theory of the Gunn effect, Proc. IEEE 52 (1964) 1736.
[6] R.E. Goldwasser, High-performance second-harmonic operation W-band GaAs gunn diodes, IEEE Electron. Device Lett. 10 (1989) 412–414, https://doi.org/10.1109/55.34726.
[7] H. Eisele, R. Kamoua, Submillimeter-wave InP Gunn devices, IEEE Trans. Microw. Theor. Tech. 52 (2004) 2371–2378, https://doi.org/10.1109/TMTT.2004.835974.
[8] A.S. Hajo, O. Yilmazoglu, B. Samodi, A. Dadgar, F. Kuppers, T. Kussorow, A new approach to achieve Gunn effect for GaN based THz sources with high power; A new approach to achieve Gunn effect for GaN based THz sources with high power, in: 44th International Conference on Infrared, Millimeter, and Terahertz Waves, IRMMW-THz), 2019.
[9] E. Alekseev, D. Pavlidis, GaN Gunn diodes for THz signal generation, IEEE MTT-S International Microwave Symposium Digest 3 (2000) 1905–1908, https://doi.org/10.1109/mwsym.2000.862354.
[10] M. Montes, G. Dunn, A. Stephen, A. Khalid, C. Li, D. Cumming, C.H. Oxley, R. H. Hopper, M. Kuball, Reduction of impact ionization in GaAs-based planar Gunn diodes by anode contact design, IEEE Trans. Electron. Dev. 59 (2012) 654–660, https://doi.org/10.1109/TED.2011.2177094.
[11] A. Khalid, C. Li, N.J. Pilgrim, M.C. Holland, G.M. Dunn, D.R.S. Cumming, Novel composite contact design and fabrication for planar Gunn devices for millimeter-wave and terahertz frequencies, Phys. Status Solidi (C) Current Topics in Solid State Physics 8 (2011) 316–318, https://doi.org/10.1002/pssc.201000529.
[12] P.H. Siegel, THz Technology: an Overview, 2003. www.worldsclentitic.com.
[13] H.W. Hsu, M.J. Dominguez, V. Sih, Gunn threshold voltage characterization in GaAs devices with wedge-shaped tapering, J. Appl. Phys. 128 (2020), https://doi.org/10.1063/5.0016101.
[14] S.H. Chung, Gunn Laser, Ph.D, University of Essex, 2005.
[15] N.J. Pilgrim, A. Khalid, C. Li, G.M. Dunn, D.R.S. Cumming, Contact shaping in planar Gunn diodes, Phys. Status Solidi (C) Current Topics in Solid State Physics 8 (2011) 313–315, https://doi.org/10.1002/pssc.201000539.
[16] A. Redo-Sanchez, N. Laman, B. Schulkin, T. Tongue, Review of terahertz technology readiness assessment and applications, J. Infrared, Millim. Terahertz Waves 34 (2013) 500–518, https://doi.org/10.1007/s10762-013-9998-y.
[17] C. Cetinkaya, S. Mutlu, O. Donmez, A. Erol, Characterization of emitted light from travelling Gunn domains in $Al_{0.08}Ga_{0.92}As$ alloy based Gunn devices, Superlattice. Microst. 111 (2017) 744–753, https://doi.org/10.1016/j.spmi.2017.07.028.
[18] S.A. Mohd Akhbar, D.S. Ong, Analysis of notch-δ-doped GaAs-based Gunn diodes, J. Phys. D Appl. Phys. 55 (2022), https://doi.org/10.1088/1361-6463/ac767c.
[19] P.D. Southgate, Recombination processes following impact ionization by high-field domains in gallium arsenide, J. Appl. Phys. 38 (1967) 4589–4595, https://doi.org/10.1063/1.1709190.
[20] N. Balkan, M. Hostut, Transient studies of light emission from travelling space charge domains in GaAs and $Ga_{1-x}Al_xAs$, Physica B 272 (1999) 291–294.
[21] S. Chung, N. Balkan, Fabry-perot gunn laser, Appl. Phys. Lett. 86 (2005) 1–2, https://doi.org/10.1063/1.1937995.
[22] N. Balkan, S.H. Chung, Micro-cavity surface emitting Gunn laser, in: Proceedings of 2005 7th International Conference on Transparent Optical Networks, ICTON, 2005, pp. 97–101, https://doi.org/10.1109/ICTON.2005.1506107, 2005.
[23] C. Li, Design and Characterisation of Millimetre Wave Planar Gunn Diodes and Integrated Circuits High Frequency Electromagnetic Measurements and Modelling of Extreme Impedance Devices View Project, 2012. http://theses.gla.ac.uk/.
[24] S.A. W.H.-H, W. Kowalsky, Transferred-electron domains in $In_{0.53}Ga_{0.47}As$ in dependence on the the nl product, Solid State Electron. 27 (1984) 187–189.
[25] M.A. Haase, V.M. Robbins, N. Tabatabaie, G.E. Stillman, Subthreshold electron velocity-field characteristics of GaAs and $In_{0.53}Ga_{0.47}As$, J. Appl. Phys. 57 (1985) 2295–2298, https://doi.org/10.1063/1.335464.
[26] B.K. Ridley, Specific Negative Resistance in Solids, 1963.
[27] Sze S.M. K.K.Ng, Physics of Semiconductor Devices, Third Edition, A. John Wiley & Sons, Inc., 2007.
[28] C. Canali, C. Forzan, A. Neviani, L. Vendrame, E. Zanoni, R.A. Hamm, R.J. Malik, F. Capasso, S. Chandrasekhar, Measurement of the electron ionization coefficient at low electric fields in InGaAs-based heterojunction bipolar transistors, Appl. Phys. Lett. (1995) 1095, https://doi.org/10.1063/1.113583.
[29] R.K. Ahrenkiel, R. Ellingson, S. Johnston, M. Wanlass, Recombination lifetime of $In_{0.53}Ga_{0.47}As$ as a function of doping density, Appl. Phys. Lett. 72 (1998) 3470–3472, https://doi.org/10.1063/1.121669.
[30] M. Hostut, N. Balkan, Light Emission from Travelling Space Charge Domains, 1999.

Already have a manuscript?

Use our Manuscript Matcher to find the best relevant journals!

Find a Match

Filters Clear All

Web of Science Coverage

Open Access

Category

Country / Region

Language

Frequency

Journal Citation Reports

Refine Your Search Results

Materials Science in Semiconductor Processing

Search

Sort By: Relevancy

Search Results

Found 21,865 results (Page 1) Share These Results

Exact Match Found

MATERIALS SCIENCE IN SEMICONDUCTOR PROCESSING

Publisher: **ELSEVIER SCI LTD , 125 London Wall, London, England, EC2Y 5AS**

ISSN / eISSN: **1369-8001 / 1873-4081**

Web of Science Core Collection: **Science Citation Index Expanded**

Additional *Web of Science* Indexes: **Current Contents Electronics & Telecommunications Collection | Current Contents Engineering, Computing & Technology | Current Contents Physical, Chemical & Earth Sciences | Essential Science Indicators**

Share This Journal

View profile page

** Requires free login.*

Other Possible Matches